International Journal of Heat and Fluid Flow 52 (2015) 64–71

Contents lists available at ScienceDirect

International Journal of Heat and Fluid Flow

journal homepage: www.elsevier.com/locate/ijhff

Parametric perturbative study of the supercritical cross-flow boundary layer

Francesca De Santi [a], Stefania Scarsoglio [a], William O. Criminale [b], Daniela Tordella [a,*]

[a] Department of Mechanical and Aerospace Engineering, Politecnico di Torino, Torino 10129, Italy
[b] Department of Applied Mathematics, University of Washington, Seattle, WA 98195-2420, USA

ARTICLE INFO

Article history:
Received 28 March 2014
Received in revised form 4 October 2014
Accepted 19 November 2014

Keywords:
Boundary layers
Cross-flow
Initial value problem
Parametric study
Travelling waves

ABSTRACT

A linear analysis of the transient evolution of small perturbations in the supercritical FSC cross-flow boundary layer is presented. We used the classical method based on the temporal evolution of individual three-dimensional travelling waves subject to near-optimal initial conditions and considered an extended portion of the parameter space. Our parametrization included the wave-number, the wave-angle, the cross-flow angle, the Hartree parameter and the Reynolds number. Special focus was given to the role played by the waveangle in inducing very steep initial transient growths in waves that proved to be stable in the long term.

We found that the angular distribution of the asymptotically unstable waves and of the waves that show a transient growth depends greatly on the value of the cross flow angle and wave-angle as well as on the sign of the Hartree parameter, but depend much less on the Reynolds number. In the case of the decelerated boundary layer, at sufficiently short wavelengths, transient growths become much more rapid than the initial growth of the unstable waves. In all cases of transient growth, pressure perturbations at the wall are not synchronous with the kinetic energy of the perturbation.

We present a comparison with the sub-critical results obtained by Breuer and Kuraishi (1994) ($Re = 500$, sweep angle of $\pi/4$) for the same full range of the obliquity angle here considered (π radiants).

1. Introduction

The cross flow boundary layer is one of the most important boundary layers in engineering applications (aerospace, mechanical, wind...), cf. the recent review by Saric et al. (2003) and the monographs Schmid and Henningson (2001), Criminale et al. (2003). Examples of cross flow boundary layer include flow over a swept back air plane wing, rotating discs, cones and spheres and cones at an angle of attack. It is important to understand the dynamics of this flow and to learn how to prevent the possibility of breakdown to turbulence. Furthermore, unlike the well-known Blasius boundary layer, breakdown is far more likely in this flow. For example, it can be unstable inviscidly as well as that caused by the influence of viscosity due to the existence of an inflexion point in the mean profile (Gregory et al., 1955). This work presents a study in an extended portion of the parameter space of the stability of the cross flow boundary layer in supercritical conditions with three-dimensional perturbations based not only on the modal approach but also examining the temporal evolution of the perturbation. Flow due to an infinite rotating discs often has been used in literature as an archetypal example of three-dimensional boundary layers (Saric et al., 2003). Lingwood (1995) found that in this flow a transition from local linear convective to radial absolute instability can occur. This inspired many authors and led to the investigation of the fully non linear regime (see, among others Pier (2003), Healy (2006)).

The swept-wing boundary layer is genuinely three-dimensional, which makes its exploration very complex. Despite this complexity, Lingwood's approach motivated studies on the possibility of absolute instability operating in the swept-wing boundary layer. In particular, it was found (Lingwood, 1997) that close to the attachment line there is chordwise absolute instability above a critical spanwise Reynolds number of about 545. Taylor and Peake (1998) extended the study by Lingwood and searched for pinch points in the cross flow direction for a larger range of flow angles and pressure gradients. Although these crossflow-induced pinch points do not constitute an absolute instability, as there is no concomitant pinch occurring in the streamwise wavenumber plane, they can be used to find the maximum local growth rate contained in a wavepacket travelling in any given direction. Recently, these findings were confirmed by Koch (2002) in a work dedicated to the study of the secondary instability of stationary cross-flow vortices. In general,

* Corresponding author.
E-mail address: daniela.tordella@polito.it (D. Tordella).

http://dx.doi.org/10.1016/j.ijheatfluidflow.2014.11.007
0142-727X/

a rigorous proof that the absolute instability cannot occur in a swept-wing boundary layer does not yet exist.

The three-dimensional boundary layer has been also investigated in the context of receptivity and transient optimal perturbations. Most studies of optimal disturbances in wall-bounded flows (Luchini and Bottaro, 1998; Luchini, 2000) deal with temporal growth of perturbations. For example, Corbett and Bottaro (2001) performed a local stability analysis using a variational technique in the temporal framework. They found that the three-dimensional boundary layer shows significantly greater capacity for algebraic growth than the two-dimensional boundary layer with the same base flow parameters. Moreover, they proved that the cross flow angle that maximizes the transient growth is nearly equal to 49°. Schrader et al. (2009) and Tempelmann et al. (2010) studied the receptivity problem for spatial growing perturbation considering vortical free stream modes, free stream turbulence and surface roughness. They found that steady cross-flow instabilities to dominate for low-level free stream disturbance. Malik et al. (1994, 1999) investigate the secondary instability characteristics of swept-wing boundary and found that three types of secondary disturbances can be distinguished. The first two were high-frequency disturbances with high growth rates and maxima located away from the wall. Their origin was related to regions of high spanwise shear (type I) and vertical shear (type II). The third type is a low-frequency disturbance with smaller growth rates and maxima closer to the wall representing a primary travelling crossflow disturbances being modulated by the stationary crossflow vortex.

This work treats the linear perturbation problem and demonstrates the importance of the results during the transient period as well the long time behaviour. Near-optimal perturbations which are localized within the boundary layer thickness are used as initial conditions (Lasseigne et al., 1999; Corbett and Bottaro, 2001). We also have good agreement with results obtained by using impulsive forcing (Taylor and Peake, 1998) or least-damped Orr–Sommerfeld eigenfunctions as initial conditions (Breuer and Kuraishi, 1994). The extreme simplicity of this method allows for an extended study of the parameter space. In particular, special attention was given to the role played by the direction of the perturbation both in the transient and in the asymptotic regime. In sub-critical conditions, a similar analysis was performed by Breuer and Kuraishi (1994). They observed that, when the external flow is accelerated, the disturbances which have greater transient growth are those that propagate in the crossflow direction. Vice versa, if the external flow is decelerated, the maximum transient growth is obtained with disturbances propagating in the opposite cross-flow direction.

With this paper we wish to extend the study of Breuer and Kuraishi by considering supercritical conditions. The pressure perturbation during the transient is also investigated and in particular is investigated when the maximum amplification factor for the pressure measured at the wall come in advance or in delay with respect to the maximum amplification of the energy.

This paper is organized as follow. The physical problem is described in Section 2. Section 2.1 is dedicated to the mean three-dimensional flow, Section 2.2 to the definition of the initial value problem and modal analysis. Sections 3 and 4 present transient dynamics and the role of the perturbation inclination and the long term behaviour, respectively. Section 5 gives information on the wall pressure transient. Conclusions follow in Section 6.

2. Problem formulation

2.1. Mean flow

As customary, we use the parallel flow approximation to describe the linear evolution of small amplitude disturbances. When the parallel flow assumption holds, the base flow components only vary with the wall normal coordinate. The assumption behind this approach is that the mean boundary layer flow quantities vary slowly in the streamwise direction compared to the disturbance quantities. In general, to account for nonparallel effects in diverging flows, the spatial formulation of the governing perturbative equations is used, see for example the multiple scale analysis carried out by El-Hady (1991) who considers the nonparallel effects for subsonic and supersonic boundary layers. A specific application to the base flow analysed in this paper (the Falkner–Skan–Cooke boundary layer, with a displacement thickness Reynolds number of 490) can be found in Högberg and Henningson (1998) where, by means of linear local eigenvalue calculations compared to spatial direct numerical simulations, it is showed that nonparallel effects induce a raise in the growth rate of the order of the 13% along the streamwise direction.

In this paper, nonparallels effect are disregarded. We thus assume that locally we can represent the boundary layer as a parallel shear flow subject to small pertubations in the form of travelling waves and define two local coordinate systems as shown in Fig. 1(a) and (b). On an infinite swept wing, taken any point x^* lying on the wing, we can always distinguish the chordwise direction, x_c, from the streamline direction, x. We use the coordinate system based on the streamline direction. The y direction is normal to the wall and the z direction is normal to both x and y directions. A good approximation of the velocity profiles in a three dimensional boundary layer is given by the family of similarity solutions known as Falkner–Skan–Cooke (FSC) solutions (Cooke, 1950; Rosenhead, 1963). There are two parameters in the FSC formulation that allow the magnitude of the cross flow to be varied: β, the dimensionless pressure gradient, or Hartree parameter, and θ the crossflow angle between the streamwise direction and the chordwise direction, see Fig. 1(c). The mean vertical velocity is assumed to be zero.

It should be recalled that with this approximation the external flow is accelerating as the external pressure decreases ($\beta > 0$) and one can talk of boundary layer in a favourable pressure gradient and vice versa.

Fig. 1(b) and (c) shows the velocity profiles in this reference frame. As is customary, variables are non-dimensionalized with respect to U_e, the free-stream velocity at the boundary layer edge, and with respect to the streamwise displacement thickness, $\delta^* = \int_0^\infty (1-U)dy$. The Reynolds number is then defined as $Re = U_e\delta^*/\nu$.

2.2. Initial-value problem and modal analysis

The transient as well as the long term behaviours of arbitrary three-dimensional disturbances acting on the FSC cross-flow boundary layer are investigated. We have considered the velocity vorticity formulation and have Fourier transformed the governing disturbance equations in the streamwise and spanwise directions only, using respectively the wavenumbers α and γ. This leads to generalized forms of the Orr–Sommerfeld and Squire equations:

$$\begin{aligned} &\left(\tfrac{\partial}{\partial t} + i(\alpha U + \gamma W)\right)\left(\tfrac{\partial^2}{\partial y^2} - k^2\right)\hat{v} - i(\alpha U'' + \gamma W'')\hat{v} - \tfrac{1}{Re}\left(\tfrac{\partial^2}{\partial y^2} - k^2\right)^2 \hat{v} = 0, \\ &\left[\tfrac{\partial}{\partial t} + i(\alpha U + \gamma W) - \tfrac{1}{Re}\left(\tfrac{\partial^2}{\partial y^2} - k^2\right)\right]\hat{\omega}_y = i(\alpha W' - \gamma U')\hat{v}, \end{aligned} \quad 3, \quad (1)$$

where $k^2 = \alpha^2 + \gamma^2$ is the polar wavenumber, $\hat{v}$ and $\hat{\omega}_y$ are respectively the transformed perturbation vertical velocity and vorticity, U, U', U'', W, W' and W'' indicate the base flow streamwise and spanwise profiles and their derivatives in the y direction. The boundary conditions require that $\hat{v} = \hat{v}' = \hat{\omega}_y = 0$ at the wall and at infinity.

On these equations we have performed both a modal analysis and an initial value problem, which hereafter will be indicated

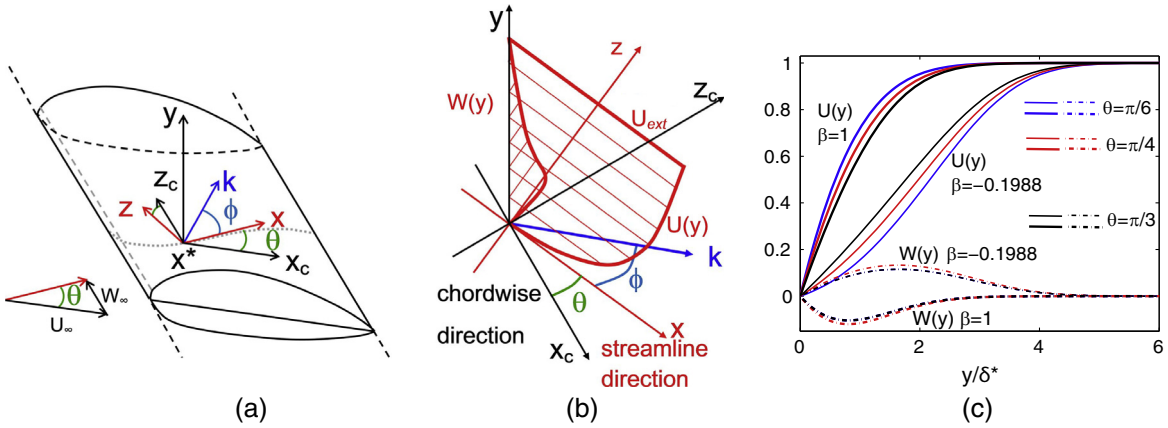

Fig. 1. Scheme: (a) Chordwise (x_c, y, z_c) and streamline (x, y, z) reference frame. The cross flow angle, θ, is represented in green; the perturbation propagation is represented in blue. k is the polar wavenumber and ϕ is the wave-angle. The attachment line is shown as a dashed line, the external streamline is indicated by the dotted line. (b) 3D of the boundary layer velocity profiles, $U(y)$ and $W(y)$. (c) Solutions of the Falkner Skan Cooke flow. Effect of changing the parameters: $\beta = -0.1988, 1$ and $\theta = \pi/6, \pi/4, \pi/3$. Note that $W(y;\beta,\theta) \propto \sin\theta\cos\theta$ (Cooke, 1950), as a consequence $W(y;\beta,\theta=\pi/3) = W(y;\beta,\theta=\pi/6)$. (For interpretation of the references to colour in this figure legend, the reader is referred to the web version of this article.)

with the abbreviation IVP. In the modal analysis to compute the eigenvalues, $\sigma = \sigma_r + i\sigma_i$, of Eq. (1) a finite differences scheme of the fourth order of accuracy is used. In the IVP we have adopted the method of lines (Scarsoglio et al., 2009; Scarsoglio et al., 2010; Lasseigne et al., 1999). This approach offers an alternative means for which arbitrary initial conditions can be specified and the full temporal behaviour, including both early-time transients and the long-term asymptotics, can be observed.

For the temporal evolution, to measure the growth of the perturbations we define the kinetic energy density:

$$e(t;k,\phi,\beta,\theta,Re) = \frac{1}{2}\int_0^{y_f} \left(|\hat{u}|^2 + |\hat{v}|^2 + |\hat{w}|^2\right) dy, \tag{2}$$

where y_f is the computational limit of the domain, while $\hat{u}(y,t;k,\phi,\beta,\theta,Re)$, $\hat{v}(y,t;k,\phi,\beta,\theta,Re)$ and $\hat{w}(y,t;k,\phi,\beta,\theta,Re)$ are the transformed velocity components of the perturbation. ϕ is the wave-angle, defined as the angle between the streamwise and the perturbation directions, $\phi = \arctan(\gamma/\alpha)$, see Fig. 1(a) and (b). y_f is defined so that the numerical solutions are insensitive to further extensions of the computational domain size. We also introduce the amplification factor G, as the kinetic energy normalized with respect to its initial value:

$$G(t;k,\phi,\beta,\theta,Re) = e(t;k,\phi,\beta,\theta,Re)/e(0;k,\phi,\beta,\theta,Re). \tag{3}$$

Assuming that the temporal asymptotic behaviour of the linear perturbations is exponential, the temporal growth rate, r, that corresponds to the imaginary part of the modal analysis eigenvalue, can be defined as

$$r(t;k,\phi,\beta,\theta,Re) = \log(e(t;k,\phi,\beta,\theta,Re))/(2t). \tag{4}$$

The frequency, ω, of the perturbation is defined as the temporal derivative of the wave phase, φ, at a specific spatial point along the y direction. The wrapped phase, φ_w is a discontinuous function of t defined in $[-\pi, +\pi]$, while the unwrapped phase, φ, is a continuous function obtained by introducing a sequence of 2π shifts on the phase values in correspondence to the periodical discontinuities. The frequency (Whitham, 1974; Scarsoglio et al., 2009) is thus

$$\omega(t;y_0,k,\phi,\beta,\theta,Re) = |d\varphi(t;y_0,k,\phi,\beta,\theta,Re)|/dt. \tag{5}$$

This corresponds to the real part of the modal analysis eigenvalue. As reference, we use the transversal observation point $y_0 = 1$, i.e. $y_0 = \delta^*$.

It should be noted that when r and ω become constant, the asymptotic state is reached. In the asymptotic limit, in respect to the modal analysis, the IVP can only select the mode which has the largest growth rate.

We have considered supercritical flows (Re = 1000–7000) subject to both positive and negative external pressure gradients ($\beta = -0.1988, 1$). The cross flow angle, θ, is taken in the range $[\pi/12, 11\pi/25]$. Concerning the perturbations, we vary both the polar wavenumber, k, and the wave-angle ϕ. For the IVP, as initial condition, we use a Gaussian distribution for the velocity field, while the vorticity is initially zero, namely

$$v(0) = y^2 exp(-y^2), \qquad \omega_y(0) = 0. \tag{6}$$

We recall that y is normalized on the displacement thickness based on the streamwise velocity, see Section 2.1. However, in order to make some comparison with literature data (Breuer and Kuraishi, 1994), in Section 3 we have performed simulations with different initial condition at $Re = 500$ and $\beta = 0.2$.

To validate the numerical procedure, solutions obtained by both the modal approach and the IVP are compared with each other and with data in literature; cf. Fig. 2. In both cases, Fig. 2(a) shows good agreement with the results of Taylor and Peake (1998) ($\gamma = 0.35 + i0.125$, Fig. 5 therein). Since we have not found any discrete and continuous spectra for the cross flow boundary layer to compare with, in Fig. 2(b) we have considered as base flow the Blasius boundary layer and contrasted our results with Mack (1976).

3. Transient dynamics and role of the obliquity angle

As mentioned in the introduction we want to extend the results of Breuer and Kuraishi (1994) to the case of supercritical flow. As initial condition they use the least-damped Orr–Sommerfeld eigenfunction for the velocity field and set the vertical vorticity equal to zero. See in Fig. 3(a) the comparison between their initial condition extending outside the boundary layer and the initial condition defined in Eq. (6). Breuer and Kuraishi consider stable waves and found that transient growth can be observed in a narrow range of wavenumbers ($k \in [0.2, 1.1]$). Within this region, they observe that for positive β, positive values of ϕ show a greater transient growth than those with negative values, see Fig. 3(c), and the peak value is achieved for an obliquity angle of about 80° ($9/20\pi$). For negative value of β, the opposite is true and the peak value is reached for an obliquity angle of about −80°.

To further validate our simulations we have done some simulation using their initial condition, as done also by Corbett and

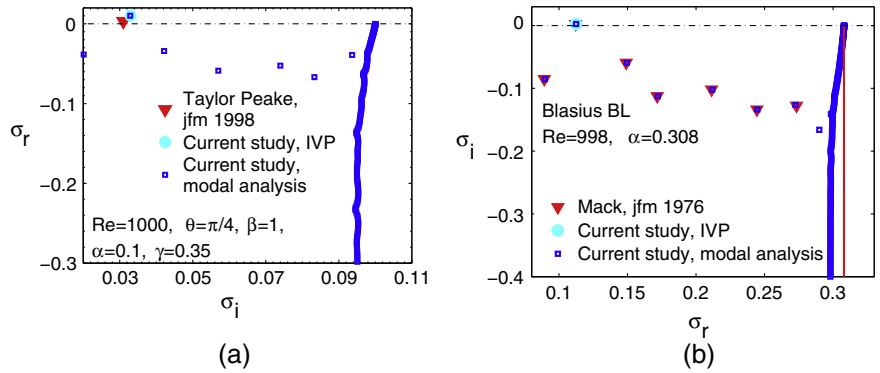

Fig. 2. Spectra of eigenvalues of the Orr–Sommerfeld equation. Comparison of different numerical methods: 4th order finite differences scheme (blue squares); initial value problem (cyan circles); literature data (red triangles). (a) Cross flow boundary layer $Re = 1000, \beta = 1, \theta = \pi/4, \alpha = 0.01, \gamma = 0.35, \nabla$ Taylor and Peake (1998), same parameters but complex spanwise wavenumber ($\gamma = 0.35 + i0.125$). (b) Blasius boundary layer flow, $Re = 998, k = 0.308, \phi = 0, \nabla$ Mack (1976). Please note that with our approach the continuous part of the spectrum is discretely approximated. The red line represents the analytical solution obtained by taking $\hat{v}$ and $\hat{v}'$ bounded for $|y| \to \infty$. (For interpretation of the references to colour in this figure legend, the reader is referred to the web version of this article.)

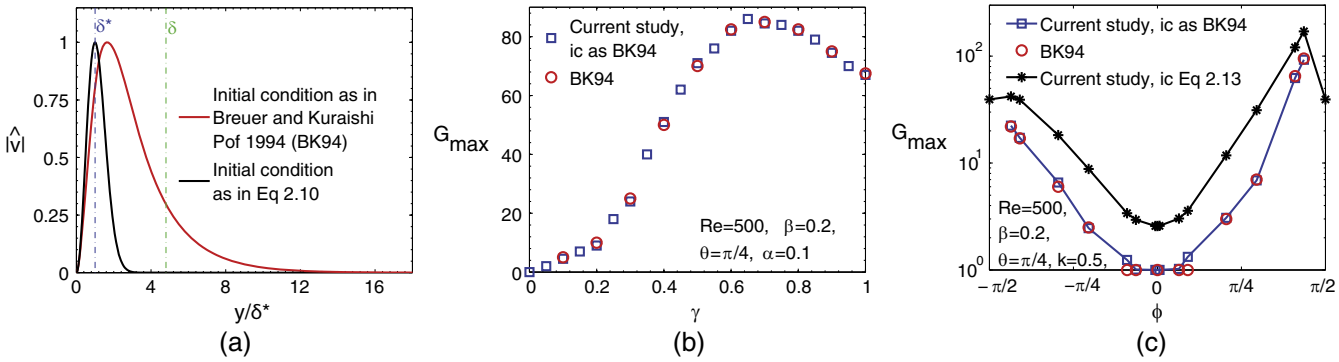

Fig. 3. Comparison between the current study and Breuer and Kuraishi (BK94). (a) Their (red) and our (black) initial condition profile. Vertical dash-dotted lines indicate the displacement thickness and the boundary layer width. (b–c) Numerical results at $Re = 500, \beta = 0.2$ and $\theta = \pi/4$. Red circles indicate results from BK94, green triangles show results by Corbet and Bottaro (CB01), blue squares are the reproduction of results in BK94 made with our numerical procedure using their initial condition, black asterisks are the transient growths obtained by the initial condition Eq. (6). (b) Maximum of the amplification factor as a function of the spanwise wavenumer with $\alpha = 0.1$ and initial condition as in BK94. (c) Maximum of the amplification factor as a function of the the obliquity angle at $k = 0.5$. Results in CB01 are obtained at $\theta = 48.8$ using an optimal initial condition. (For interpretation of the references to colour in this figure legend, the reader is referred to the web version of this article.)

Bottaro (2001) (see Fig. 3 therein), getting a very good agreement, see blue squares in Fig. 3(b) and (c). In Fig. 3(c), the transient growth obtained with the initial condition (6) is again contrasted with Breuer and Kuraishi results. We also have a point of comparison with an optimal perturbation at a similar sweep angle (48.8°) obtained by Corbet and Bottaro. It should be noted that according to Lasseigne et al. (1999) and Corbett and Bottaro (2001), our kind of initial condition fully confined within the boundary layer promotes the initial energy gain. However, in this study we are not focusing on the use of optimal initial conditions, but we simply wish to describe how in supercritical condition the obliquity of arbitrary perturbation can influence its evolution.

Fig. 4 shows the temporal evolution of the amplification factor for perturbation with different obliquity angles at the supercritical Reynolds number of 5000. Fixing the wavenumber, when the external flow is accelerated, the growth rate increases with the positive wave-angle up to $\phi = 5/12\pi$ and then slightly decreases, see Fig. 4(a), while for negative angles the increase is monotonic, see Fig. 4(d). One can also note that in case of transient growth the maximum of G is monotonically increasing with the modulus of ϕ. When the external flow is decelerated a rather general rule can be found. When considering positive angles of obliquity, Fig. 4(b) and (c), $k = 0.4$) highlights a rich and, for certain aspects, counter-intuitive scenario on the role of the perturbation direction. We see in fact that the waves with small obliquity together with the orthogonal waves are unstable but a range of oblique waves in between are not. Usually, in 2D shear flows, if one sees instability in the longitudinal direction, one then sees a progressive tendency to stability moving toward the orthogonal direction. Instead, here, intermediate angles have an intense initial growth and then become stable. When considering negative angles of obliquity, Fig. 4(e) and (f), we see that the waves do not present significant transient growth and are all unstable. It should be noted that for the cases in panels (a–c) in Fig. 4, the polar wavenumber vector of perturbations beyond $\phi = \pi/3$ has negative chordwise component (i.e. $\theta + \phi > \pi/2$). We can introduce the phase velocity, defined as $\mathbf{C} = (\omega/k)\hat{\mathbf{k}}$, where $\hat{\mathbf{k}}$ is the unitary vector in the k direction, and we can observe that the travelling waves with a phase velocity propagating toward the attachment line of the wing are unstable for $\beta = 1$ and are transiently growing for $\beta = -0.1988$. However the energy of the perturbations is transported by the group velocity, $v_g = (d\omega/d\alpha, d\omega/d\gamma)$, that propagates in the positive chordwise direction (see for example the values reported in Table 1).

4. Long-term behaviour

Regarding the influence of the wave-angle on the long-term behaviour, the best way to study it is by means of the modal analysis. In fact, considering the large number of parameters involved, with the IVP the knowledge of the final growth rate of

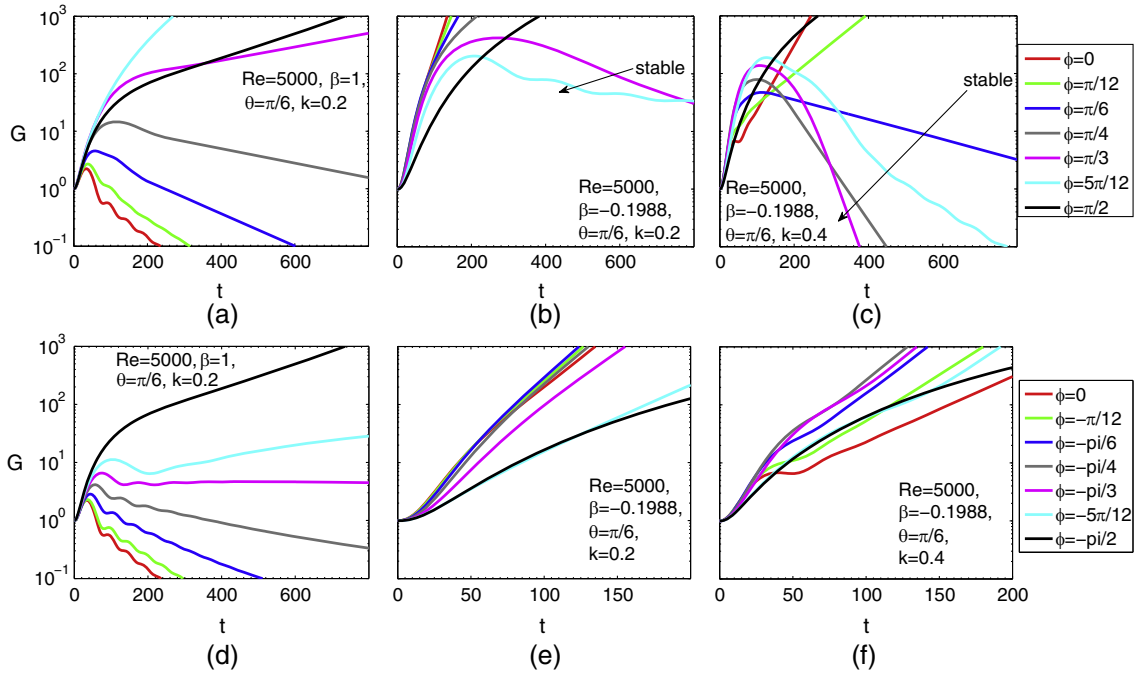

Fig. 4. Temporal evolution of the amplification factor, $G(t)$ for perturbations with different obliquity angles, $\phi = 0, \pi/12, \pi/6, \pi/4, \pi/3, 5\pi/12, \pi/2$ at $Re = 5000$ and $\theta = \pi/6$. Left panel $\beta = 1$, middle and right panels $\beta = -0.1988$. Panels (a, b, d and e) $k = 0.2$, panels (c and f) $k = 0.4$

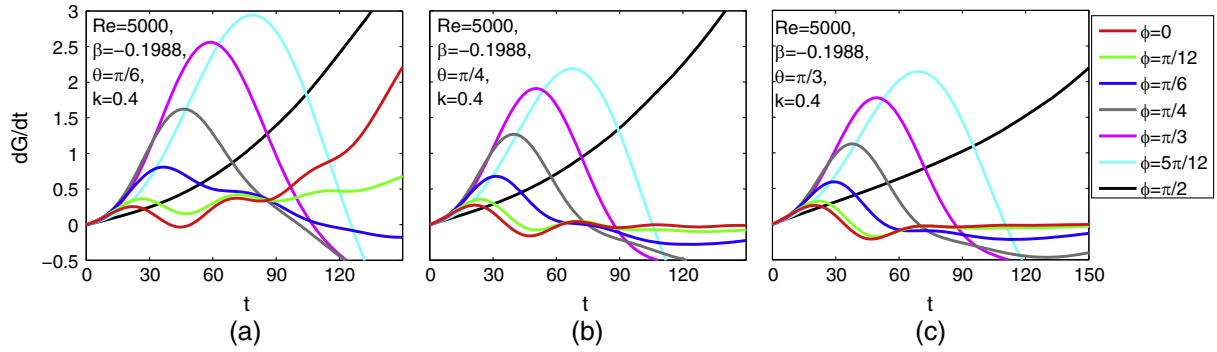

Fig. 5. Temporal evolution of the amplification factor growth, $dG(t)/dt$ for perturbations with different obliquity angles, $\phi = 0, \pi/12, \pi/6, \pi/4, \pi/3, 5\pi/12, \pi/2$ at $Re = 5000, \beta = -0.1988$ and $k = 0.4$. Panel (a), $\theta = \pi/6$. Panel (b), $\theta = \pi/4$. Panel (c), $\theta = \pi/3$.

Table 1
Examples of group velocity at the temporal asymptote: variation with the central wavenumber of the wave packet k_0. FSC boundary layer with Hartree parameter 1 and −0.1988 and $Re = 5000, \theta = \pi/4, \phi = 5\pi/12$. The increment Δk is 0.002.

$\beta = 1$		
k_0	$v_{g_x} = d\omega/d\alpha$	$v_{g_y} = d\omega/d\gamma$
0.02	0.2994	0.0802
0.04	0.2855	0.0765
0.2	0.3249	0.0871
0.4	0.4007	0.1074
1.2	0.9992	0.2677
1.4	0.9995	0.2678
$\beta = -0.1988$		
0.02	0.4841	0.1297
0.04	0.4331	0.1161
0.2	1.0320	0.2765
0.4	1.0316	0.2764
1.2	1.0366	0.2778
1.4	1.0455	0.2801

a perturbation would require a large computational effort and a large memory space to store the temporal results (there are simulations that can last up to 10^5 time scales). In Fig. 6 the growth rate is shown for different combination of obliquity angle, pressure gradient and cross-flow angle and two different wavenumbers taken in the range of the most unstable one. r is computed as the imaginary part of the least damped eigenvalue in the discrete spectrum Taylor and Peake (1998) have also investigated the combined effect of β and θ. Considering wavenumbers supporting pinch points, they found that asymptotically the perturbations acting on an adverse pressure gradient base flow are more unstable at lower cross flow angles, while for negative pressure gradient the opposite is true. Our results are completely in agreement with their observations.

Summarizing the situation shown in Fig. 6, by changing the sign of Hartree's parameter, the sign of the growth rate changes. A concentration of the growth factor values that become nearly constant in the range $[-\pi/3, \pi/3]$ is observed for the accelerated boundary layer at $k = 0.4$, see Fig. 6(c). A less intense similar trend is

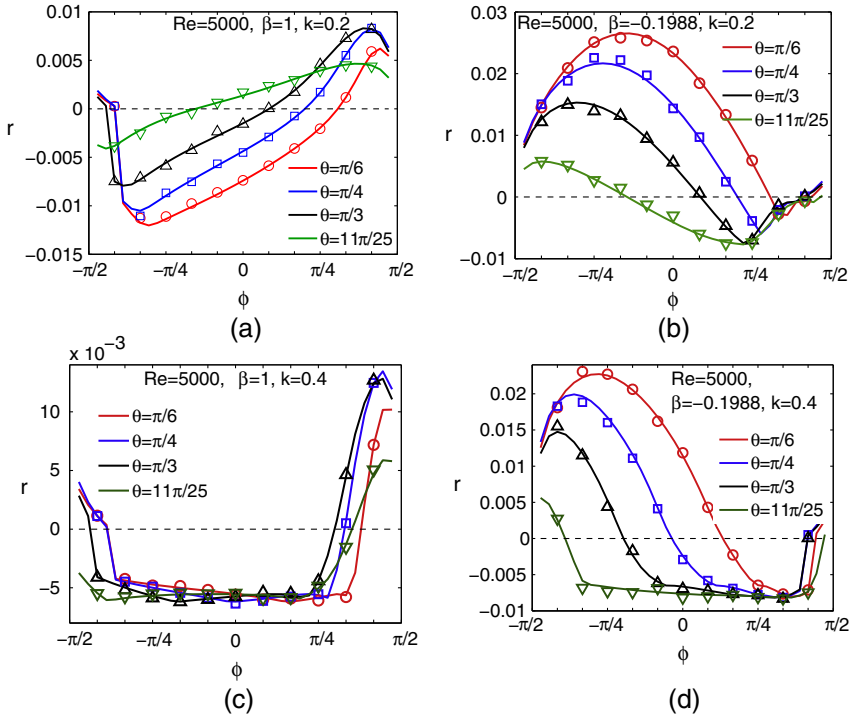

Fig. 6. Growth rate as a function of the obliquity angle for different cross flow angles. Circle, triangles and squares are values computed by the IVP and reported here to further validate the numerical results.

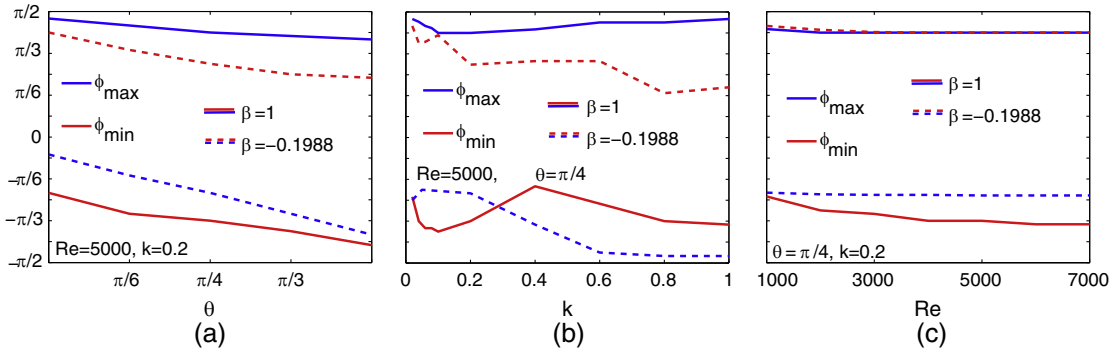

Fig. 7. ϕ_{min} and ϕ_{max}, obliquity angle for which the growth rate reaches respectively its minimum negative value and its maximum positive value, as a function of the base flow and the perturbation parameters. Solid lines $\beta = 1$, dashed lines $\beta = -0.1988$. Panel (a), dependency on the cross flow angle at $Re = 5000, k = 0.2$. Panel (b), dependency on k at $Re = 5000, \theta = \pi/4$. Panel (c), trends with Re in the case $k = 0.2, \theta = \pi/4$.

observed in Fig. 6(d) for the same configuration with a positive pressure gradient.

In Fig. 7 we describe the variations of the obliquity angles for which the growth rate reaches its minimum negative value, ϕ_{min}, and its maximum positive value, ϕ_{max}. These angles are slightly decreasing with the cross flow angle, Fig. 7(a). They are almost constant with the Reynold number, Fig. 7(c), which confirms Lingwood (1997). The behaviour with the wavenumber in the range $[0.02 - 1]$ is a bit more complex as shown in Fig. 7(b). When the external pressure gradient is positive (dashed lines) ϕ_{max} and ϕ_{min} are general decreasing function of the wavenumber. For $\beta = 1$ (solid lines), both ϕ_{min} and ϕ_{max} present a local mild minimum where the waves are long ($k \approx 0.1$). Furthermore ϕ_{min} has a local maximum at $k = 0.4$.

5. Perturbed pressure transient

In literature, as regards the perturbed pressure field, effects associated with the pressure gradient on the outside are mainly considered. For example, the effects on the growth rate and propagation of turbulent spots on the wall (Seifert and Wygnanski, 1995). Little is found on the characteristics of the pressure field within the same layer and in particular on the wall. For this reason we analysed the evolution of the perturbed pressure at the wall and found a behaviour that is not easily predictable by the amplification factor evolution. The pressure field is computed by the Poisson equation, $\Delta\hat{p} = -ik(\cos(\phi)U' + \sin(\phi)W')\hat{v}$, with boundary conditions $\hat{p}(y \to \infty) = 0 \quad \hat{p}'(y = 0) = \hat{v}''(y = 0)/Re$. As in the previous section, we are primarily interested in the role of the obliquity angle. For this purpose we define the equivalent of the amplification factor for the pressure:

$$P = |\hat{p}(y = 0, t)|/|\hat{p}(y = 0, t = 0)|, \tag{7}$$

that we call pressure amplification. We consider only stable waves that have a transient energy growth. As expected, the pressure field is also initially amplified. This transient growth does not follow the amplification factor transient growth. This is illustrated in Fig. 8. Fig. 8(a) and (b) show the time evolution of the pressure

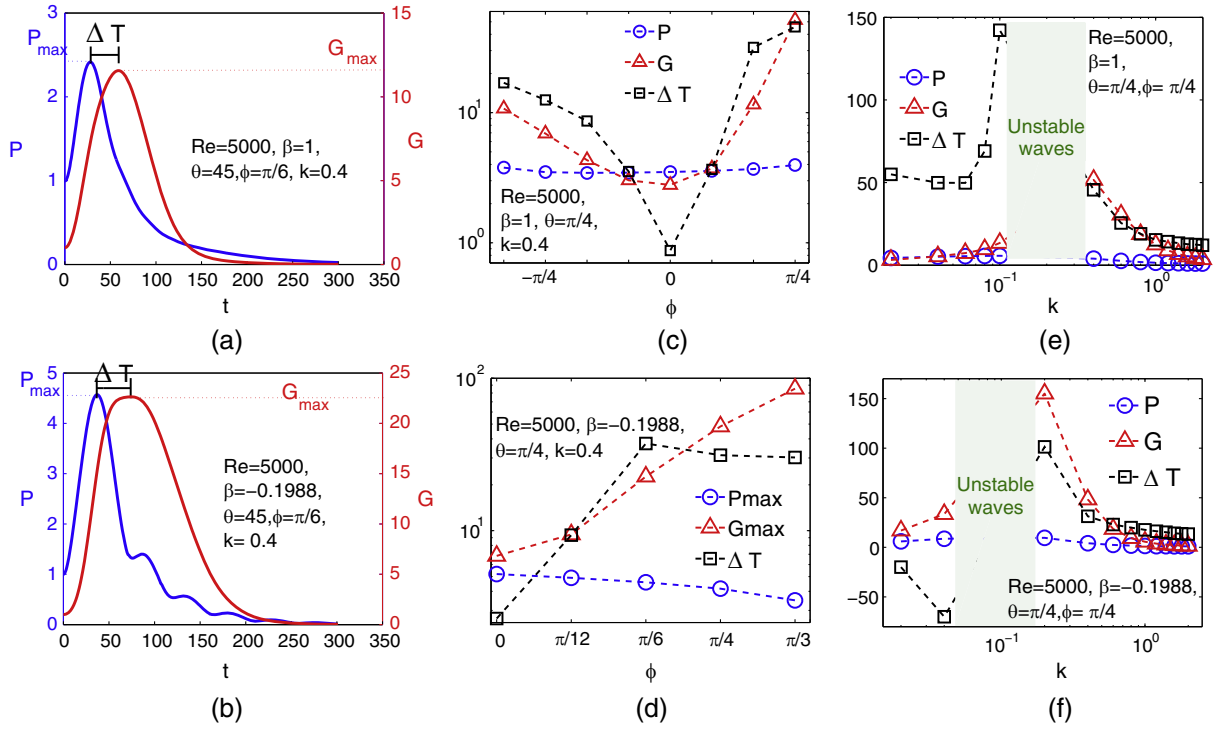

Fig. 8. Amplification factor and the pressure transients, $Re = 5000, \theta = \pi/4$, Top panels $\beta = 1$, bottom panel $\beta = -0.1988$. Left panels: examples of transient for P (Eq. (7)) and $G, k = 0.4, \phi = \pi/6$. Panels (c–f) transient of stable perturbations. Blue circles: maximum of the pressure amplification; red triangles: maximum of the amplification factor; black squares: difference between the times where the perturbation reaches G_{max} and P_{max}. Panels (c and d) role of the obliquity angle, $k = 0.4$. Panels (e and f) role of the wavenumber, $\phi = \pi/4$. (For interpretation of the references to colour in this figure legend, the reader is referred to the web version of this article.)

amplification contrasted to the time evolution of the amplification factor respectively for a favourable and an adversepressure gradient. In this last case once its maximum value is reached, the pressure has an oscillatory damping. Moreover, in this case the maximum value of the pressure amplification, P_{max}, is always higher than in the case of $\beta = 1$. In Fig. 8(c) and (d), as a function of the wave-angle, P_{max} is reported (circles) together with the maximum of the amplification factor G_{max} (triangles) and the difference between the times where the two maxima are reached $\Delta T = t(G(t) = G_{max}) - t(P(t) = P_{max})$ (squares). We can observe that P_{max} decreases with the obliquity angle for $\beta = -0.1988$ while it increases with the module of ϕ in the other case. In the case of favourable pressure gradient, Fig. 8(c), we also observe that all the quantities increase with the obliquity angle. Instead for negative β, P_{max} decreases with ϕ while G_{max} grows. ΔT does not have a monotone behaviour: increases initially, reaches a maximum at $\phi = \pi/6$ and then decreases. We also investigated the role of the wavenumber in this context. Fig. 8(e) and (f) show the transient growths as a function of the polar wavenumber for waves with obliquity angle and cross flow angle $\pi/4$. For $\beta = 1$ all the quantities, P_{max}, G_{max} and ΔT grow with the wavenumber if k is below the range of instability and decrease otherwise, see Fig. 8(e). For $\beta = -0.1988$, Fig. 8(f), highlights a different possible behaviour. In fact all the travelling waves shown in Fig. 8 have positive ΔT, but the very long waves in panel *(f)* ($k < 0.05$) have negative ΔT. In this cases the maximum of P can be delayed with respect to the maximum of G for waves longer than those in the unstable range. Even if it is not graphically presented here, we have observed that in general P_{max} and G_{max} both increase with θ for negative β and decrease with θ for positive β. The pressure behaviour here described at the wall also holds throughout the entire boundary layer.

6. Concluding remarks

In this work we present a comprehensive study of the space of the parameters relevant to the life of small perturbations of the three-dimensional boundary layer in cross flow. We considered a group of five parameters: the Reynolds number, the external pressure gradient, the wave number, the angle of cross flow and the tilt of the perturbation with respect to the streamline of the flow outside the boundary layer. We adopted almost optimal initial conditions and classical perturbation methods to obtain information on initial transient and temporal long-term behaviour.

We compared our results with results produced by other numerical simulations concerning the evolution of three-dimensional perturbations. In particular for the long term behaviour we compare our results with Taylor and Peake (1998) and Mack (1976), while for the initial transient we compare our results with Breuer and Kuraishi (1994) and Corbett and Bottaro (2001). In both cases good agreement was found.

Perturbations that have transitional growth but are asymptotically stable could still have a substantial role in triggering non-linear processes that may lead to transition to turbulence. Some of our results are related to this role, in particular with respect to the influence of the wave-angle. We show that in the decelerated three-dimensional boundary layer at a high Reynolds number there are some asymptotically stable perturbations in the range of wave-angles $[20 - 75]$ which are initially able to grow up to six times faster than those which are asymptotically unstable (waves almost aligned with the external flow or orthogonale to it). Among these, some have negative phase speeds, that is they propagate in the negative chordwise direction, although the associated group velocities are always positive and the energy propagates in the positive direction. This was observed for Reynolds

numbers based on the displacement thickness higher than 10^3, which means Reynolds numbers of the order of 10^4 or 10^7, respectively, when calculated on the thickness of the layer or on a chord of the wing profile of about one meter.

There are two other noticeable aspects. The first is that in the decelerated three-dimensional boundary layer the most unstable perturbations are either those nearly aligned with the external current or those almost orthogonal to it, that is almost aligned with the cross flow. Oblique perturbations in between always have strong growths which, however, are still transient, while the perturbations with tilt and direction of propagation opposite to the cross flow are all unstable.

The second aspect is that the perturbed field of pressure at the wall and inside the layer is not synchronous with the amplification factor of the kinetic energy of the disturbances. In general, in the case of boundary layers both accelerated and decelerated, the perturbed pressure field is made in advance up to about 100 times scale. However, in the decelerated case, it is also observed that the very long wave perturbations can induce a significant delay in the oscillation of the pressure which again may be approximately up to 100 time scales of the system.

Acknowledgment

We acknowledge the CTR Foundation and the Lagrange Project for supporting our research (www.progettolagrange.it/en/strumenti/index.html). In particular, for granting the PhD scholarship to F.D.

References

Breuer, K.S., Kuraishi, T., 1994. Transient growth in two and threedimensional boundary layers. Phys. Fluids 6, 1983–1993.
Cooke, J.C., 1950. The boundary layer of a class of infinite yawed cylinders. Proc. Camb. Phil. Soc. 46, 645–?648.
Corbett, P., Bottaro, A., 2001. Optimal linear growth in swept boundary layers. J. Fluid Mech. 435, 1–23.
Criminale, W.O., Jackson, T.L., Joslin, R.D., 2003. Theory and Computation of Hydrodynamic Stability. Cambridge University Press.
El-Hady, N.M., 1991. Nonparallel instability of supersonic and hypersonic boundary layers. Phys. Fluids 3 (9), 2164–2178.
Gregory, N., Stuart, J.T., Walker, W.S., 1955. On the stability of three-dimensional boundary layers with application to the flow due to a rotating disk. Philos. Trans. Roy. Soc. London. Series A, Math. Phys. Sci., 155–199.
Healy, J.J., 2006. A new convective instability of the rotating-disk boundary layer with growth normal to the disk. J. Fluid Mech. 560, 279–310.
Högberg, M., Henningson, D., 1998. Secondary instability of cross-flow vortices in Falkner Skan Cooke boundary layers. J. Fluid Mech. 368, 339–357.
Koch, W., 2002. On the spatio-temporal stability of primary and secondary crossflow vortices in a three-dimensional boundary layer. J. Fluid Mech. 456, 85–111.
Lasseigne, D.G., Joslin, R.D., Jackson, T.L., Criminale, W.O., 1999. The transient period for boundary layer disturbances. J. Fluid Mech. 381, 89–119.
Lingwood, R.J., 1995. Absolute instability of the boundary layer on a rotating disk. J. Fluid Mech. 299, pp. 17-17.
Lingwood, R.J., 1997. Absolute instability of the Ekman layer and related rotating flows. J. Fluid Mech. 331, 405–428.
Luchini, P., 2000. Reynolds-number-independent instability of the boundary layer over a flat surface: optimal perturbations. J. Fluid Mech. 404 (1), 289–309.
Luchini, P., Bottaro, A., 1998. Görtler vortices: a backward-in-time approach to the receptivity problem. J. Fluid Mech. 363, 1–23.
Mack, L.M., 1976. A numerical study of the temporal eigenvalue spectrum of the Blasius boundary layer. J. Fluid Mech. 73, 497–520.
Malik, M.R., Li, F., Chang, C.-L., 1994. Crossflow disturbances in three-dimensional boundary layers: nonlinear development, wave interaction and secondary instability. J. Fluid Mech. 268, 1–36.
Malik, M.R., Li, F., Chang, C.-L., 1999. Secondary instability of crossflow vortices and swept-wing boundary-layer transition. J. Fluid Mech., 399 85–399115.
Pier, B., 2003. Finite-amplitude crossflow vortices, secondary instability and transition in the rotating-disk boundary layer. J. Fluid Mech. 487, 315–343.
Rosenhead, L., 1963. Laminar Boundary Layers: An Account of the Development, Structure, and Stability of Laminar Boundary Layers in Incompressible Fluids, Together with a Description of the Associated Experimental Techniques. Clarendon Press.
Saric, W.S., Reed, H.L., White, E.B., 2003. Stability and transition of three-dimensional boundary layers. Annu. Rev. Fluid Mech. 35, 413–440.
Scarsoglio, S., Tordella, D., Criminale, W.O., 2009. An exploratory analysis of the transient and long-term behavior of small three-dimensional perturbations in the circular cylinder wake. Stud. Appl. Math. 123, 153–173.
Scarsoglio, S., Tordella, D., Criminale, W.O., 2010. Role of long waves in the stability of the plane wake. Phys. Rev. E 81, 036326.
Schmid, P.J., Henningson, D.S., 2001. Stability and Transition in Shear Flows. Springer.
Schrader, L., Brandt, L., Henningson, D.S., 2009. Receptivity mechanisms in three-dimensional boundary-layer flows. J. Fluid Mech. 618, 209–241.
Seifert, A., Wygnanski, I.J., 1995. On turbulent spots in a laminar boundary layer subjected to a self-similar adverse pressure gradient. J. Fluid Mech., 296 185–296 210.
Taylor, B.J., Peake, N., 1998. The long-time behaviour of incompressible swept-wing boundary layers subject to impulsive forcing. J. Fluid Mech. 355, 359–381.
Tempelmann, D., Hanifi, A., Henningson, D.S., 2010. Spatial optimal growth in three-dimensional boundary layers. J. Fluid Mech. 646, 5–37.
Whitham, G., 1974. Linear and Nonlinear Waves. Wiley-Interscience.